Visualizing sodium dynamics in isolated cardiomyocytes using fluorescent nanosensors

J. Matthew Dubach[a], Saumya Das[b,c], Anthony Rosenzweig[b], and Heather A. Clark[a,1]

[a]Biomedical Engineering Group, The Charles Stark Draper Laboratory, 555 Technology Square, Cambridge, MA 02139; and [b]Cardiovascular Institute, Beth Israel Deaconess Medical Center, 330 Brookline Avenue Boston, MA 02215; and [c]Cardiac Arrhythmia, Cardiovascular Division, Massachusetts General Hospital, 55 Fruit Street, Boston, MA 02114

Edited by Robert Langer, Massachusetts Institute of Technology, Cambridge, MA, and approved August 06, 2009 (received for review May 28, 2009)

Regulation of sodium flux across the cell membrane plays a vital role in the generation of action potentials and regulation of membrane excitability in cells such as cardiomyocytes and neurons. Alteration of sodium channel function has been implicated in diseases such as epilepsy, long QT syndrome, and heart failure. However, single cell imaging of sodium dynamics has been limited due to the narrow selection of fluorescent sodium indicators available to researchers. Here we report, the detection of spatially defined sodium activity during action potentials. Fluorescent nanosensors that measure sodium in real-time, are reversible and are completely selective over other cations such as potassium that were used to image sodium. The use of the nanosensors in vitro was validated by determining drug-induced activation in heterologous cells transfected with the voltage-gated sodium channel $Na_V1.7$. Spatial information of sodium concentrations during action potentials will provide insight at the cellular level on the role of sodium and how slight changes in sodium channel function can affect the entirety of an action potential.

cellular imaging | ion channels | sodium sparks

Voltage-gated sodium channels (VGSC) are transmembrane proteins that tightly regulate Na^+ fluxes across the membrane of excitable cells. The large Na^+ concentration gradient across the membrane requires only transient channel openings for sufficient Na^+ flux to rapidly depolarize the membrane. The membrane depolarization then leads to an orchestrated opening of other voltage-gated ion channels that comprises the action potential. Entry of Ca^{2+} during the action potential serves as a second messenger for further calcium release, excitation-contraction coupling, or neurotransmitter release. Hence, even minor alterations in VGSC function and kinetics can have drastic effects on cellular functions. Accordingly, mutations in the cardiac-specific VGSC have been shown to underlie diseases such as atrial fibrillation, long QT syndrome, cardiomyopathies, and Brugada syndrome (1), while mutations in the neuronal isoforms have been linked to epilepsy and pain disorders (2–4).

VGSC function and Na^+ fluxes have been studied by methods such as patch clamp (5) and voltage-sensitive dye staining (6, 7). These studies have provided information about steady-state ion channel functions and increased our knowledge of channel structure-function correlations in heterologous expression systems but provide no spatial information. Molecular fluorescent indicators for sodium designed for intracellular sodium measurements (8) have failed to provide the extraordinary results associated with similar fluorescent indicators for calcium, such as the detection of sparks in both resting and electrically stimulated cardiomyocytes (9–11). To achieve sodium concentration spatial resolution in cardiomyocytes, sensors need to have minimal response time and high sodium selectivity. Hence, development of methods of investigating real-time sodium fluxes in cytoarchitectural complex cells, such as cardiomyocytes, will significantly advance our understanding of the role of Na^+ fluxes in cellular function.

Optode-based sensors for intracellular ion measurements have been previously explored (12). We have previously developed fluorescent nanosensors for sodium that have properties designed for intracellular measurements (13). Briefly, the nanosensors have ideal response characteristics for the measurement of intracellular sodium and are exquisitely selective for Na^+ over K^+. Selectivity for Na^+ over K^+ is critical when performing intracellular measurements, because the background K^+ concentration is an order of magnitude higher than that of sodium. They are roughly 120 nm in diameter and have poly(ethylene) glycol coating to impart solution stability and biocompatibility. The properties of these probes have been studied in a cell-free solution, but their performance in vitro had not been explored until this report.

Results and Discussion

Patch Clamp Validation of $Na_V1.7$ Activity and Determination of Nanosensor Interference. Patch clamp current-voltage experiments were performed on human embryonic kidney cells that stably express the sodium channel $Na_V1.7$ (HEK PN1) to verify channel activity. Because $Na_V1.7$ is the dominant voltage-dependent channel expressed in these cells, the current-voltage curve should be dictated by the channel activity. The peak sodium current was at −20 mv (Fig. 1*A*, black squares) which correlates to $Na_V1.7$ activity determined in other studies (14, 15). Current-voltage experiments were also performed with sodium nanosensors loaded through the patch pipet. These experiments determined if the presence of sodium sensors would alter $Na_V1.7$ activity (Fig. 1*A*, red circles) either by buffering the intracellular sodium concentration or directly acting on channel function. Membrane properties and channel activities have been shown to be affected by the presence of nanoparticles intracellularly (16). However, after correcting for the difference in liquid junction potential due to the negative zeta potential of the nanosensors (13), the peak sodium current was unchanged by the presence of the nanosensors (Fig. 1*A*). The presence of nanosensors does not alter the activity of the $Na_V1.7$ sodium channel or buffer sodium dynamics.

Loading and Calibrating Nanosensors in HEK PN1 Cells. Nanosensors were loaded into HEK PN1 cells using pressure controlled microinjection (Fig. 1*B*). This technique has been previously used to deliver small molecules to the cytoplasm of cells (17). Each injection was ≈100 pL of total volume, which correlates to 10^4 nanosensors per cell (Fig. S1). This amount provided good signal intensity but was a small enough volume to prevent damage to the cells. The nanosensors dispersed throughout the cytosol and did not aggregate near the nucleus, as seen with

Author contributions: J.M.D., S.D., A.R., and H.A.C. designed research; J.M.D. performed research; J.M.D. and S.D. analyzed data; and J.M.D., S.D., A.R., and H.A.C. wrote the paper.

The authors declare no conflicts of interest.

This article is a PNAS Direct Submission.

[1]To whom correspondence should be addressed. E-mail: hclark@draper.com.

This article contains supporting information online at www.pnas.org/cgi/content/full/0905896106/DCSupplemental.

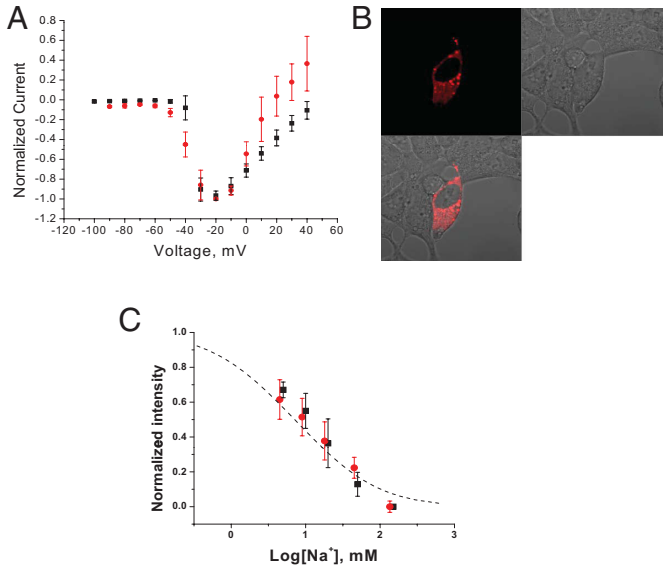

Fig. 1. Intracellular sodium measurements. (*A*) IV response curve of whole-cell patched HEK PN1 cells. Normalized sodium current using control internal filling solution (black squares) and internal filling solution containing sodium nanosensors (red circles). Data represent five experiments plus standard deviation. (*B*) HEK PN1 cell loaded with sodium nanosensors using microinjection. Confocal image showing fluorescence (633/680 nm), bright field and overlay. Single wavelength imaging was performed to achieve the fast acquisition rates required for spark detection in subsequent cardiomyocyte studies. (*C*) Concentration calibration of nanosensors in vitro (black squares) and in cell-free solution (red circles). Data represent an average of three separate experiments plus standard deviation. The theoretical curve, as described in reference 12, is plotted as well (dashed line).

endocytotic loading. Additionally, we did not see any sensor leakage or compartmentalization throughout the course of experiments.

To determine if the nanosensors responded to intracellular sodium changes in vitro similarly to responses in cell-free solutions, we calibrated the sensors once they were loaded into the HEK PN1 cells. In vitro calibrations were performed by superfusing loaded cells with varying concentrations of sodium in the presence of 5 μM gramicidin, which allows equilibration of intracellular sodium to extracellular concentrations, while maintaining solution ionic balance with potassium. This technique has been used to calibrate sodium fluorescent molecular indicators in neurons (18). Potassium was chosen, as it is the most prominent intracellular cation and has been shown to shift molecular indicator responses to sodium. The sodium concentration was increased stepwise from zero to 150 mM and back to zero, to ensure stability of the sensors throughout the experiment (Fig. S2). The plateau values for each sodium concentration were found, and the average was plotted against the sodium concentration (Fig. 1*C*). A sigmoidal curve was fit using the Hill equation, and the K_d of the nanosensors in vitro was determined to be 12 mM. Concurrently, in separate experiments, we calibrated the nanosensors in 96-well plates using a plate reader at the same wavelengths as the in vitro microscope calibrations. The same calibration solutions were used but did not include gramicidin. The average response was plotted similarly to the in vitro data, and the K_d in cell-free solution was found to be 10 mM (Fig. 1*C*). This indicates that nanosensors have the same response properties in vitro as they do in cell-free solution. Therefore, sodium nanosensors will be able to accurately measure sodium concentrations in vitro in the presence of potassium with response properties that can be determined in cell-free solution.

Measurement of Sodium Concentration Change in Response to Sodium Flux Through Voltage-Gated Channels. The HEK PN1 cells used here stably express $Na_V1.7$, which is activated by veratridine and is inhibited by multiple compounds in a dose-dependent manner (19). This provides an ideal way to control sodium channel activity in a known system to determine the efficacy of using sodium nanosensors to measure in vitro sodium dynamics. Nanosensor-loaded cells were superfused with veratridine at different concentrations to build a dose-response curve. The change in fluorescent intensity of the nanosensors in response to veratridine $Na_V1.7$ channel activation was monitored. A dose-dependent response was seen both in the rate of initial response to veratridine addition and the total, steady state response (Fig. 2*A*).

We chose to analyze the initial rate of response since the time-course of veratridine activation is rapid and transient (20), and it most emulates the channel activity during action potentials in cardiomyocytes. Therefore, we analyzed the response over the first 30 s and fit a linear curve, the best fit, to each concentration dose (Fig. 2*B*). A sigmoidal curve was fit to the initial response using the Hill equation, and the IC_{50} for veratridine response was determined to be 50 μM (Fig. 2*C*). Previous studies using HEK PN1 cells have reported an IC_{50} for veratridine of 7.7 μM using voltage sensitive dyes (19). In another cell line, the direct measurement of $^{22}Na^+$ influx through $Na_V1.7$ resulted in an IC_{50} for veratridine of 83 μM (21). The IC_{50} was larger when measuring sodium directly than using voltage-sensitive dyes, which may be due to other ions affecting voltage measurements. Therefore, because we were measuring sodium, the IC_{50} was expected to be higher than that obtained with voltage sensitive dyes in the same cell line. We compared our results to the response of the molecular dye CoroNa green to veratridine induced sodium concentration changes (Fig. S3). We were unable, however, to generate a dose-response curve using CoroNa green, which may be due to dye leakage from the cell as has been previously shown with molecular dyes (22).

Additionally, inhibition of veratridine-induced sodium concentrations by a channel inhibitor was monitored. Sodium concentration changes induced by 100 μM veratridine were measured in the presence of tetrodotoxin (TTX) at different concentrations. TTX is a specific inhibitor of $Na_V1.7$ and other sodium channels, with an IC_{50} in the nanomolar range (23). The response was normalized, and the linear slope of the initial 30 s was determined as above. These data were normalized and plotted against the concentration of TTX (Fig. 2*D*). The IC_{50} of TTX inhibition was found to be 26 nM using the Hill equation. Previous experiments using these cells found IC_{50} values of 45 and 20 nM using voltage sensitive dyes and patch clamp, respectively (19). These results validate the use of sodium nanosensors to measure intracellular sodium changes during VGSC activity.

Sodium Measurements in Isolated Cardiomyocytes. Cardiomyocytes in culture can be depolarized to initiate an action potential, and thereby generate sodium flux using field electrical stimulation. We injected isolated neonatal rat cardiomyoctyes with nanosensors as done with HEK PN1 cells. The nanosensors had a fairly even distribution throughout the cytosol with no nuclear loading. The cardiomyocytes were more sensitive to the injection of solution than the HEK PN1, which may be due to the cytoarchitecture of the myocytes. Some cells responded to injection by immediate blebbing (≈20%), however these cells were omitted from studies. The cells were imaged in a chamber that had parallel electrodes for whole field voltage stimulation. Applying a voltage gradient across the chamber activated the sodium channels and caused an action potential, which in turn stimulated excitation-contraction in the isolated cardiomyocytes. This has been a well-studied method of cardiomyocyte action potential

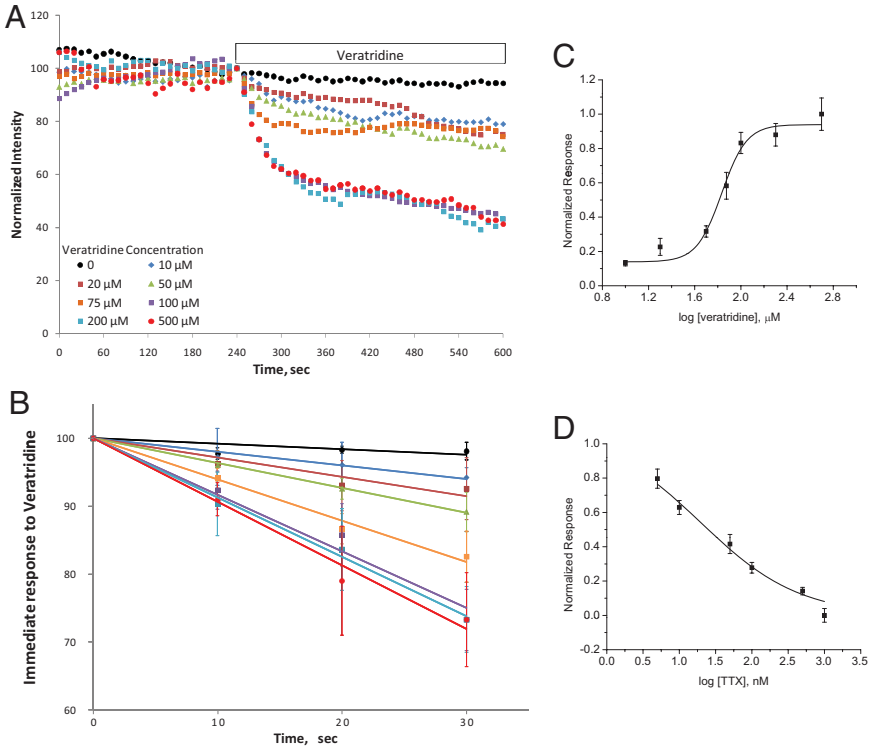

Fig. 2. Channel activation and inhibition. (*A*) Response of sodium nanosensor loaded HEK PN1 cells to veratridine. Normalized intensity of region of interest measured over time. Data represent three experiments, error not shown for clarity. (*B*) Initial linear response of veratridine addition taken from part (*A*). Dose-dependent response of nanosensor intensity and linear curve fits. Data represent three experiments with standard deviation. Veratridine concentrations are color-coded to the legend in (*A*). (*C*) Sigmoidal curve fit of linear slope response to veratridine. Data are taken from part (*B*), $n = 3$ plus standard deviation. (*D*) TTX inhibition of veratridine response. Shown are the normalized values on linear slope change dependent on TTX concentration, $n = 3$ plus standard deviation.

initiation (24–26). We applied this voltage gradient at different frequencies during experiments to pace the cells at the desired frequency. To record fluorescent images, the beating of the cardiomyocytes was inhibited. To decouple excitation and contraction, 2,3-butanedione monoxime (BDM) was applied to the cells, ensuring that motion artifacts were not contributing to signal. We found that BDM took 15 to 20 min to arrest contraction completely. To limit the depth of fluorescent detection and allow for images that measured sodium only at the membrane, the Airy unit of the pinhole was set to less than one, and the plane of focus was set at the top of the cardiomyocyte.

The channel open time of voltage-gated sodium channels during action potentials is on the order of single milliseconds. The acquisition time of the fluorescent signal must therefore be reduced so that multiple images can be acquired within the channel opening event to visualize the transient sodium concentration change. To accomplish this, two-dimensional images were acquired to find a section of the cytosol with uniform nanosensor distribution. A line was then fit across this region, and a line scan was acquired with a scanning frequency of 300–350 Hertz. A line scan allows for three acquisitions per second without losing the integrity of the spatial information by binning the image. Acquisitions were carried out over 5 to 7 s, while the cardiomyocytes will simultaneously electrically paced to produce action potentials using voltage gradients at the desired frequency.

We recorded the signal intensity of the nanosensors in the line scan and plotted it against time, an example plot is shown in Fig. 3*A*. Sodium concentration changes are brief and transient, indicating that we are measuring the voltage-gated sodium channels that open at the onset of action potentials instead of slow sodium channels or sodium concentration changes caused by the sodium-calcium exchanger. The data demonstrate spatially-dependent sodium concentration changes throughout the cell as some regions in the plot show no signal change, while others have an easily detectable sodium concentration change. Previous studies have shown that sodium channel distribution and density are not uniform in neurons (27, 28), and channel clustering occurs in cardiomyocytes (29). The occurrence of spatially-dependent sodium concentration changes is likely due to the clustering of voltage-gated sodium channels at the membrane of the cardiomyocytes.

Each point in the line scan was plotted to determine if changes in sodium concentration were measured. Some points in the line scan showed no variation in signal intensity over time, while others showed sharp spikes of increased sodium concentration, as shown in Fig. 3*B* (decreases in fluorescent signal correlate to increases in sodium concentration). We took the fast Fourier transform of the data that show sodium concentration changes and found the dominant frequency in the signal to be 1.6 Hz. The dominant frequency is the beating frequency of the cells and was faster than the pacing frequency of this experiment (1.5 Hz). To determine why a difference in pacing frequency and beating frequency was seen, cardiomyocytes were paced at frequencies from 0.5 to 2.5 Hz. Fig. 3*C* shows that the beating frequency of the cardiomyocytes remains between 1.5 and 1.7 Hz until the pacing frequency greater than or equal to 2 Hz is applied. The beating frequency of 1.5 to 1.7 Hz is likely the intrinsic beating frequency of the cardiomyocytes, which is noted in the absence of the paralyzing drug. When the pacing frequency is below the intrinsic frequency, the cardiomyocytes will beat at the intrinsic frequency, however at higher pacing frequencies, the cardiomyocytes are overdriven and beat at the pacing frequency. Two linear curves were fit in Fig. 3*C*: A flat fit is seen when field stimulation of the cardiomyocytes is below the intrinsic frequency; and a correlated linear dependence to the pacing frequency fits when the pacing frequency is above the intrinsic frequency. This result explains the slight disparity between pacing frequency and beating frequency shown in Fig. 3 *A* and *B*.

Conclusion

Akin to the calcium sparks that have been shown to occur in isolated cardiac myocytes (9, 30), we show the possible occur-

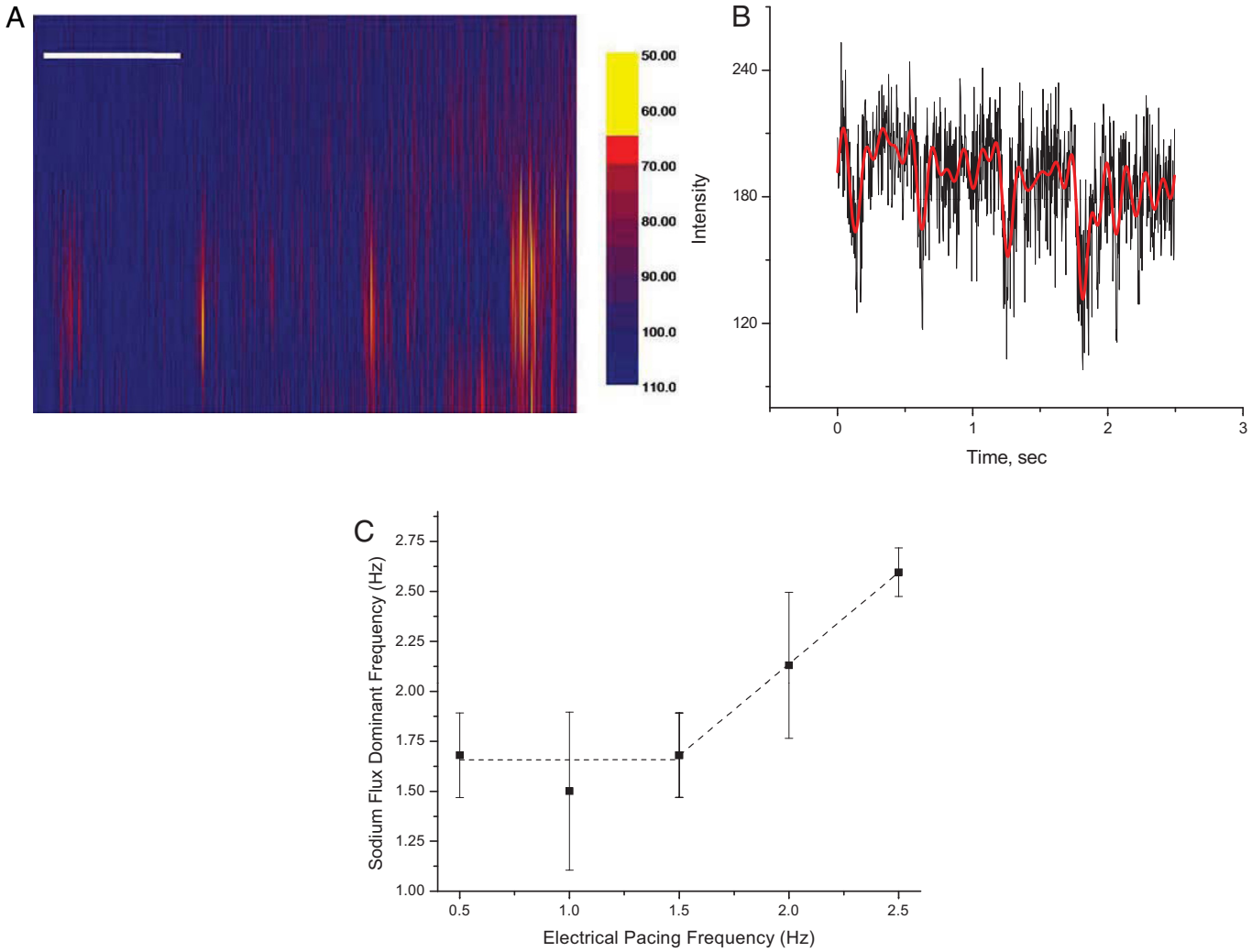

Fig. 3. Cardiac myocyte action potential. (*A*) Distance versus time plot of signal intensity for a line scan of a nanosensor-loaded, paralyzed cardiac myocyte. The intensity scale is shown on the right. Data values were determined by dividing each point scan by a linear fit over the entire time of the scan to normalize intensity values through the different points. A value of 50 indicates a 50% decrease in signal intensity from the linear fit at that point in time of the scan. The white bar represents 500 ms. (*B*) Line tracing of intensity versus time of a single spot from the line scan shown in (*A*). Shown are the raw data (black line) and 10 Hz low pass Fourier filtered data (red line). (*C*) Electrical pacing frequencies versus recorded dominant sodium flux frequency. Shown is an average of ≥3 cells plus standard deviation for each pacing frequency. Two linear fits were performed, one for the region between 0.5 and 1.5 Hz pacing frequency (below the intrinsic frequency), and the other between 1.5 and 2.5 Hz pacing frequency (a correlated fit above the intrinsic frequency).

rences of sodium sparks in the cytoplasm of cardiac myocytes. Mathematical models have been created to determine the contributions of sodium channels to the generation of an action potential in cardiac myocytes (31, 32). However, these models are unable to predict spatial distribution of sodium within the cell. Differences in location of high sodium concentrations may contribute to irregular action potentials that lead to arrhythmias in cardiomyocytes. The use of sodium selective nanosensors, described previously (13) and applied to biological measurements here, enabled spatially defined sodium concentration measurements to be performed. Additionally, the nanosensors showed efficacy in determining drug-induced activation of sodium channels. Future work will focus on the structure-function relationship of isolated cardiomyocytes and changes in sodium flux in cardiomyocytes with sodium channel mutations that are known to lead to arrhythmias.

Materials and Methods

Materials. Human embryonic kidney cells stably expressing the sodium channel hNaV1.7 (HEK PN1) were obtained from Merck. Veratridine was brought up in DMSO to 50 or 20 mM and stored at −20 °C for less than 3 months. A stock solution of TTX was made in distilled water to 1 mM or 10 μM and stored at −20 °C. Gramicidin was brought up in DMSO to 5 mM and stored at 4 °C. CoroNa green was obtained from Invitrogen, and a stock solution was made into 1-mM aliquots in DMSO and stored at −20 °C before use. All chemicals were purchased from Sigma unless otherwise noted.

Myocyte Isolation. Cardiac myocytes were prepared as previously discussed (33). Briefly, ventricular tissue harvested from postnatal day 1 rat pups was minced and subjected to enzymatic digestion with 0.4 mg/mL collagenase/0.6 mg/mL pancreatin in ADS buffer, followed by cell isolation on a Percoll gradient. Pure isolated cardiac myocytes were counted and plated at a density of 1×10^5 cells/mL on laminin-coated 25-mm glass coverslips (VWR).

Nanosensor Fabrication. The fabrication of sodium nanosensors has been previously described in detail. Briefly, a mixture consisting of the following components was brought up in tetrahydrofuran: 120 mg/mL bis(2-ethylhexyl) sebacate, 60 mg/mL high molecular weight poly(vinyl) chloride, 6 mg/mL sodium ionophore X, 2 mg/mL sodium tetrakis[3,5-bis(trifluoromethyl)phenyl]borate, and 1 mg/mL Chromoionophore III. This mixture was diluted 1:1 with dichloromethane and added to aqueous solution under probe tip sonication (Branson). The aqueous solution contained 5% (wt/vol) glucose for

injection studies or intracellular patch solution for patch clamp studies, see below, as well as 150 μg/mL 1,2-distearoyl-*sn*-glycero-3-phosphoethanolamine-N-[methoxy(polyethylene glycol)-550] (ammonium salt; Avanti Polar Lipids). After the nanosensors hardened in solution, they were filtered through a 0.2-μm syringe filter to remove larger particles. The nanosensors were used within 8 h of fabrication.

Concentration of Sensors. The concentration of the nanosensors in solution after fabrication was determined using dynamic light scattering (Zetasizer ZS90; Malvern). A standard curve was built using serial dilutions of fluospheres with a diameter of 100 nm and similar optical properties (580 nm/605 nm) in distilled water (Invitrogen). The count rate was determined for each concentration, and an average of three runs was compiled, and a curve was fit (Excel; Microsoft). Concentrations were selected to fall within the range of the count rate seen for the nanosensors. The nanosensors were then diluted in distilled water to 50%, 25%, and 10%. The count rate was determined for each dilution, and a concentration was calculated using the curve from the standard. The concentration for each dilution was then corrected for the dilution, and an average was taken. This was repeated three times using different batches of nanosensors.

Patch Clamp. Patch clamp experiments were carried out on HEK PN1 cells. Whole-cell patch clamp was performed by achieving gigaohm seals using Axopatch 200B and Digidata 1440A (Axon Instruments). Borosilicate glass pipets (Sutter Instruments) were pulled using a pipet puller (model *p*-97; Sutter) and flame polished (polisher; Narashigi) to a resistance of 2–4 MOhm in solution. Experiments were carried out 5 min after a whole-cell GOhm seal was achieved. Standard IV curve experiments were performed stepping the holding voltage from −100 to 40 mV in 10-mV increments. The data were processed using pclamp10 and an average response was generated. The external solution contained the following: 30 mM sodium chloride, 110 mM cesium chloride, 1.8 mM calcium chloride, 2 mM cadmium chloride, 1 mM magnesium chloride, 10 mM HEPES, 10 mM glucose, 1 mM 4-AP. The internal solution contained: 10 mM sodium chloride, 130 mM cesium chloride, 5 mM EGTA, 10 mM HEPES, 10 mM glucose. For nanosensor studies, they were made in the internal filling solution. The liquid junction potential of the internal filling solution with and without nanosensors was determined, and the difference was used to correct the response in the IV curves.

Imaging. Images were recorded on a Zeiss 510 meta confocal microscope. Nanosensors were imaged using a 633 nm He/Ne laser with emission at 680 ± 10 nm. Although a major advantage of using chromoionophore-based nanosensors for intracellular measurements is the ability to perform ratiometric measurements, a single wavelength was used to allow for faster acquisition rates than could be achieved using ratiometric emission recordings on our instrument. CoroNa green was excited with a 485-nm argon laser with emission near 515 nm.

Microinjection and Cell Loading. HEK cells were loaded with nanosensors using microinjection. Borosilicate glass (Sutter Instruments) was pulled using a micropipet puller (model *p*-97; Sutter Instruments) to an internal diameter of 0.5–0.7 μm. Nanosensors were back loaded into the pipet, which was mounted into a holder controlled by a micromanipulator (Burleigh). Injection pressure was controlled using a microinjector (PLI-100; Warner). The injected volume was calculated according to the manufacturer (Warner). The pressure was set to allow minimal volume injection after penetrating the membrane using a tap method. Cells were injected on the microscope stage in extracellular solution containing: 10 mM HEPES, 10 mM glucose, 135 mM sodium chloride, 3 mM potassium chloride, and 1 mM calcium chloride, pH to 7.4 with NaOH/HCl. This was performed at room temperature and the cells allowed to recover for at least 10 min. The effectiveness of injection was determined by monitoring nuclear loading, cell blebbing, and cell size. If there was any nuclear loading, cellular blebbing, or the cell was significantly larger in size before injection, a new cell was selected. HEK PN1 cells were also loaded with CoroNa green AM. The cells were loaded for 25 min at 37 °C with 5 μM dye in the extracellular solution described above. The cells were then washed twice and allowed to recover at 37 °C for 10 min. In separate experiments, CoroNa green was also picoinjected into the cells for a direct comparison to nanosensor delivery. The cells were then transferred to the microscope for imaging.

Drug Induced Activation. HEK PN1 cells were plated in glass bottom dishes (Mattek) and used at least 48 h after plating. Experiments were carried out in the extracellular solution described above. After injection, a time course experiment was run for 10 to 20 min acquiring every 10 s. Veratridine was added to the cells by an equal volume addition of twice the desired concentration. In TTX experiments, TTX was added to the extracellular solution before injection and was added to the veratridine solution at the same concentration. Regions of interest were defined (LSM510 Meta; Zeiss), and the average intensities were plotted against time. The data were normalized to generate the dose-dependent curves from which the IC_{50}s were found. The response slope of a given concentration was normalized according to: $N = (Slope_{max} - Slope_{[drug]})(Slope_{max} - Slope_{min})$.

Nanosensor Calibration. In vitro calibration was performed using a gravity perfusion system. Solutions were made from stock solutions containing: 10 mM HEPES, 10 mM glucose, 1 mM calcium chloride, and either 150 mM sodium chloride or potassium chloride. The solutions were adjusted to a pH of 7.4 using Trizma base. The solutions were combined at different ratios to create the desired sodium concentration while maintaining ionic balance. Gramicidin was added to a final concentration of 5 μM. Calibration in cell-free solution was performed by diluting the nanosensors 1:10 in the sodium calibration solutions used for the in vitro calibrations. The sensors were loaded into an optical bottom 96-well plate in triplicate per concentration. The concentration of the solution was slightly lower in the calibration in cell-free solution because of dilution factors. The fluorescence was read in a plate reader exciting the sensors at 633 nm and collecting emission at 680 nm (Spectramax M2; Molecular Devices). The intensity of a given concentration was normalized according to: $\alpha = (I_{max} - I_{[Na^+]})(I_{max} - I_{min})$, where I_{max} is the intensity of the nanosensors at zero sodium, I_{min} is the intensity at 150 mM sodium, and $I_{[Na^+]}$ is the intensity at the concentration of interest. The response data, α, were plotted against the log of the sodium concentration, in mM, with the log of zero sodium set to −2 for curve fit analysis. Sigmoidal curves were fit (OriginLab) to the data, and the K_d was calculated using the software.

Myocyte Pacing. Cells were not used until at least 48 h after harvesting. The coverslips were mounted into a perfusion chamber that contained parallel electrodes running down each side (Warner Instruments). The cells were bathed in a Tyrode's solution containing the following: 130 mM sodium chloride, 5 mM potassium chloride, 10 mM glucose, 10 mM HEPES, 1 mM magnesium chloride, and 2 mM calcium chloride, pH to 7.4 using NaOH/HCl. Additionally, 20 mM 2,3-Butanedione monoxime was added. The chamber was mounted on the microscope and attached to a voltage generator (ECM 830; Harvard Apparatus). Microinjection of the sensors was performed as described previously. The cells were then paced using a 30-V gradient for 5 ms at 1 Hz. If beating was seen, the injected cell was determined to be viable. The cells were then allowed to sit for 10 min to allow the decoupling of the excitation and contraction to occur due to the presence of 2,3-Butanedione monoxime. An image was then acquired, and a line scan was performed on a region containing nearly uniform sensor distribution. Line scan images were then acquired at greater than or equal to 300 Hz, depending on the line scan length, while pacing the cells. Data were assessed as a two-dimensional plot, time versus distance in the x direction, and analyzed for beat patterns at each distance point. Data were plotted as a matrix of intensity values with time and direction as the axes. Individual spot scans were plotted, and a Fourier 10-Hz low pass filter was applied to smooth the response (OriginLab). A fast Fourier transform was applied to determine the dominant frequency (OriginLab). The average dominant frequency for each pacing frequency was determined and plotted.

ACKNOWLEDGMENTS. We thank Dr. Owen Mcmanus of Merck and Prof. Norbert Klugbauer of Albert-Ludwigs-Universität Freiburg for providing the HEK PN1 cells; Drs. Jeremy Ruskin and Patrick Ellinor for their thoughtful suggestions; and Drs. Ling Li and Chunyang Xiao for technical help with myocyte preparations. This work was supported by National Institutes of Health National Institute of General Medical Sciences Grant R01 GM084366; Draper Internal Research and Development; a Leducq Foundation Network of Research Excellence, Judith and David Ganz, and the Maxwell Hurston Charitable Foundation (to A.R.); and the Harvard-MIT Health Sciences and Technology Clinical Investigation Training Program grant and National Institutes of Health/National Heart, Lung, and Blood Institute Grant K08 HL081319 (to S.D.).

1. Clancy CE, Rudy Y (2002) Na(+) channel mutation that causes both Brugada and long-QT syndrome phenotypes: A simulation study of mechanism. *Circulation* 105:1208–1213.
2. Cox JJ, et al. (2006) An SCN9A channelopathy causes congenital inability to experience pain. *Nature* 444:894–898.
3. Drenth JP, Waxman SG (2007) Mutations in sodium-channel gene SCN9A cause a spectrum of human genetic pain disorders. *J Clin Invest* 117:3603–3609.
4. Meisler MH, Kearney JA (2005) Sodium channel mutations in epilepsy and other neurological disorders. *J Clin Invest* 115:2010–2017.
5. Kim DY, et al. (2007) BACE1 regulates voltage-gated sodium channels and neuronal activity. *Nat Cell Biol* 9:755–764.
6. Huang CJ, et al. (2006) Characterization of voltage-gated sodium-channel blockers by electrical stimulation and fluorescence detection of membrane potential. *Nat Biotechnol* 24:439–446.

7. Tsutsui H, Karasawa S, Okamura Y, Miyawaki A (2008) Improving membrane voltage measurements using FRET with new fluorescent proteins. *Nat Methods* 5:683–685.
8. Minta A, Tsien RY (1989) Fluorescent indicators for cytosolic sodium. *J Biol Chem* 264:19449–19457.
9. Cheng H, Lederer WJ, Cannell MB (1993) Calcium sparks: Elementary events underlying excitation-contraction coupling in heart muscle. *Science* 262:740–744.
10. Wang SQ, Stern MD, Rios E, Cheng H (2004) The quantal nature of Ca2+ sparks and in situ operation of the ryanodine receptor array in cardiac cells. *Proc Natl Acad Sci USA* 101:3979–3984.
11. Cannell MB, Cheng H, Lederer WJ (1994) Spatial non-uniformities in [Ca2+]i during excitation-contraction coupling in cardiac myocytes. *Biophys J* 67:1942–1956.
12. Brasuel M, Kopelman R, Kasman I, Miller TJ, Philbert MA (2002) Ion concentrations in live cells from highly selective ion correlation fluorescent nano-sensors for sodium. *Proc IEEE* 1:288–292.
13. Dubach JM, Harjes DI, Clark HA (2007) Fluorescent ion-selective nanosensors for intracellular analysis with improved lifetime and size. *Nano Lett* 7:1827–1831.
14. Lampert A, Dib-Hajj SD, Tyrrell L, Waxman SG (2006) Size matters: Erythromelalgia mutation S241T in Nav1.7 alters channel gating. *J Biol Chem* 281:36029–36035.
15. Sheets PL, et al. (2006) Inhibition of Nav1.7 and Nav1.4 sodium channels by trifluoperazine involves the local anesthetic receptor. *J Neurophysiol* 96:1848–1859.
16. Tang M, et al. (2008) Unmodified CdSe quantum dots induce elevation of cytoplasmic calcium levels and impairment of functional properties of sodium channels in rat primary cultured hippocampal neurons. *Environ Health Perspect* 116:915–922.
17. Liu G, et al. (2003) Nanoparticles of compacted DNA transfect postmitotic cells. *J Biol Chem* 278:32578–32586.
18. Meier SD, Kovalchuk Y, Rose CR (2006) Properties of the new fluorescent Na+ indicator CoroNa green: Comparison with SBFI and confocal Na+ imaging. *J Neurosci Methods* 155:251–259.
19. Felix JP, et al. (2004) Functional assay of voltage-gated sodium channels using membrane potential-sensitive dyes. *Assay Drug Dev Technol* 2:260–268.
20. Saleh S, Yeung SY, Prestwich S, Pucovsky V, Greenwood I (2005) Electrophysiological and molecular identification of voltage-gated sodium channels in murine vascular myocytes. *J Physiol* 568:155–169.
21. Maruta T, et al. (2008) Lysophosphatidic acid-LPA1 receptor-Rho-Rho kinase-induced up-regulation of Nav1.7 sodium channel mRNA and protein in adrenal chromaffin cells: Enhancement of 22Na+ influx, 45Ca2+ influx and catecholamine secretion. *J Neurochem* 105:401–412.
22. Despa S, Islam MA, Pogwizd SM, Bers DM (2002) Intracellular [Na+] and Na+ pump rate in rat and rabbit ventricular myocytes. *J Physiol* 539:133–143.
23. Jo T, et al. (2004) Voltage-gated sodium channel expressed in cultured human smooth muscle cells: Involvement of SCN9A. *FEBS Lett* 567:339–343.
24. Werdich AA, et al. (2008) Differential effects of phospholamban and Ca2+/calmodulin-dependent kinase II on [Ca2+]i transients in cardiac myocytes at physiological stimulation frequencies. *Am J Physiol Heart Circ Physiol* 294:H2352–H2362.
25. del Monte F, et al. (1999) Restoration of contractile function in isolated cardiomyocytes from failing human hearts by gene transfer of SERCA2a. *Circulation* 100:2308–2311.
26. Picht E, et al. (2007) CaMKII inhibition targeted to the sarcoplasmic reticulum inhibits frequency-dependent acceleration of relaxation and Ca2+ current facilitation. *J Mol Cell Cardiol* 42:196–205.
27. Lai HC, Jan LY (2006) The distribution and targeting of neuronal voltage-gated ion channels. *Nat Rev Neurosci* 7:548–562.
28. Kole MH, et al. (2008) Action potential generation requires a high sodium channel density in the axon initial segment. *Nat Neurosci* 11:178–186.
29. Soeller C, Crossman D, Gilbert R, Cannell MB (2007) Analysis of ryanodine receptor clusters in rat and human cardiac myocytes. *Proc Natl Acad Sci USA* 104:14958–14963.
30. Lopez-Lopez JR, Shacklock PS, Balke CW, Wier WG (1995) Local calcium transients triggered by single L-type calcium channel currents in cardiac cells. *Science* 268:1042–1045.
31. Wang LJ, Sobie EA (2008) Mathematical model of the neonatal mouse ventricular action potential. *Am J Physiol Heart Circ Physiol* 294:H2565–H2575.
32. Bondarenko VE, Szigeti GP, Bett GC, Kim SJ, Rasmusson RL (2004) Computer model of action potential of mouse ventricular myocytes. *Am J Physiol Heart Circ Physiol* 287:H1378–H1403.
33. Morissette MR, et al. (2006) Myostatin regulates cardiomyocyte growth through modulation of Akt signaling. *Circ Res* 99:15–24.